# Repurposing of Some VEGFR-2 Inhibitors: In Silico Molecular Dynamics Simulation (at 200 ns), Docking Based on the SARS-CoV-2-Main-Protease Inhibitor N3

*Sanadelaslam SA El-Hddad[1]; Mohamed H Sobhy[2]; Hamada S Abulkhair[3,4]; Khaled El-Adl[2,5]\**

[1]*Pharmaceutical Chemistry Department, Faculty of Pharmacy, Omar Almukhtar University, Al Bayda 991, Libya.*

[2]*Chemistry Department, Faculty of Pharmacy, Heliopolis University for Sustainable Development, Cairo, Egypt.*

[3]*Pharmaceutical Organic Chemistry Department, Faculty of Pharmacy, Al-Azhar University, Nasr City 11884, Cairo, Egypt.*

[4]*Pharmaceutical Chemistry Department, Faculty of Pharmacy, Horus University - Egypt, International Costal Road, New Damietta, Egypt.*

[5]*Pharmaceutical Medicinal Chemistry & Drug Design Department, Faculty of Pharmacy (Boys), Al-Azhar University, Cairo11884, Egypt.*

*\*Corresponding Author: Khaled El-Adl*

*Email: khaled.eladl@hu.edu.eg*

### Abstract

The present study suggests the potential anti-SARS-CoV-2 activities of thirty five reported VEGFR-2 inhibitors containing the amide and urea linkers. Nineteen members revealed the best *in silico* results and hence, were subjected to further MD simulation for their inhibitory activities against SARS-CoV-2 M$^{pro}$ across the 200 ns. Furthermore, Molecular Dynamics (MD) simulations followed by calculation the free energy of binding were also carried out for the most promising ligand-pocket complexes from docking studies to clarify some information on their dynamic and thermodynamic properties and approve the docking results. These results we obtained probably provided an excellent lead candidate for the development of therapeutic drugs against COVID-19. Both compounds Lenvatinib (4), Nintedanib (9), 28 and 32 as VEGFR-2 inhibitors bound to SARS-CoV-2 M$^{pro}$ target have depicted significant free binding and affinity to target's pocket. These results greatly confirmed our proposed rational and matched with our computational findings through molecular docking (targeting the viral M$^{pro}$) and molecular dynamics which consequently suggest the strong expected activities for the other studied and discussed VEGFR-2 inhibitors as well.

**Keywords**: Drug repurposing; Thiazolidine-2,4-dines; Docking; COVID-19; Main protease.

### Introduction

Drug repurposing/repositioning, a strategy effectively employed in cancer treatment [1], can represent a valid alternative, provided that suitable medications are selected among the enormous number of potential, already synthesized, and often already clinically employed, compounds. Drug repurposing has already been suggested for specific drugs in the treatment of the current COVID-19 outbreak [2-7]. Most of the drugs contemplated for repurposing/repositioning the treatment of the COVID-19 outbreak are commercially available, and their doses and toxicity in humans are well known, due to clinical use for years (or even decades). This can allow their utilization in faster and less expensive phase II–III clinical trials, or even within straightforward compassionate use. In particular, a significant number of drugs that have been reevaluated for COVID-19

treatment are or have been used as anticancer agents. This should not be surprising if we consider that virus-infected cells are pushed to enhance the synthesis of nucleic acids, protein and lipid, and boost their energy metabolism, in order to comply to the "viral program". Indeed, the same features are seen in cancer cells, making it likely that drugs interfering with specific cancer cell pathways may be effective as well in defeating viral replication. In order to make a rational and effective choice of drugs amenable of repurposing for the therapy of COVID-19, we can elaborate existing data, from experimental and translational research, clinical trials, anecdotal reports and other published information. We present here a comprehensive analysis of available information on potential candidate VEGFR-2 inhibitors as cancer drugs that can be repurposed for the treatment of COVID-19.

There are four genera (α, β, γ, and δ) of corona viruses. Severe acute respiratory syndrome-related coronavirus (SARS-CoV), the Middle East respiratory syndrome coronavirus (MERS-CoV), and SARS-CoV-2 are β-coronaviruses [8]. Analysis of the genome sequences of these three viruses has revealed that SARS-CoV-2 has a higher identity to SARS-CoV (89.1% nucleotide similarity) than to MERS-CoV [9]. The genome of SARS-CoV-2 is a positive-sense single-stranded RNA of approximately 30 kb in length and at least has six open reading frames (ORFs) that code for a minimum of 16 non-structural proteins and 4 structural proteins [10]. The 229E gene encodes two polyproteins involved in functional polypeptides release, which are required for viral transcription and replication. The proteolytic-responsible protease processing is 3 chymotrypsin-like proteases of SARS-CoV-2 (3CLpro or $M^{pro}$), as it cleaves at least 11 sites on the polyproteins translated from the viral RNA [11,12]. Given the relevance for the viral replication cycle, thus the viral protease ($M^{pro}$) has been proven as an attractive target in the development of inhibitors against coronaviruses [13-18].

Currently, there is no single specific antiviral therapy for COVID-19 and the main treatments is only supportive [19]. Drug repurposing is a strategy that adopted by several researchers to seek effective treatment in a short period [20]. Besides, the hypothetical assay based on molecular docking is emerging as an essential tool to discover new antiviral agents, as researchers can use this tool as a complementary approach prior to the synthesis of new compounds [21]. While traditional methods of drug discovery could take years, the approach taken here to search for possible medications for the SARS-CoV-2 is the *in silico* screening (molecular docking and dynamics simulations) of models towards the SARS-CoV-2 $M^{pro}$ protein.

### Rational of the work

The *HIV-1* protease inhibitor, nelfinavir, strongly inhibits the replication of the SARS coronavirus (SARS-CoV). Nelfinavir inhibits the cytopathic effect induced by SARS-CoV infection [22]. Similar to nelfinavir, ritonavir and lopinavir are recommended as protease inhibitors for the treatment of SARS and MERS, which have similar mechanisms of action as on HIV [23]. *HIV-1* protease inhibitors on the one hand are structurally containing different amide and urea linkers (sequinavir, atazanvir, nelfinavir, fosamperavir, darunavir, indanavir, rotinavir and lopinavir) as depicted in Figure 1 [24].
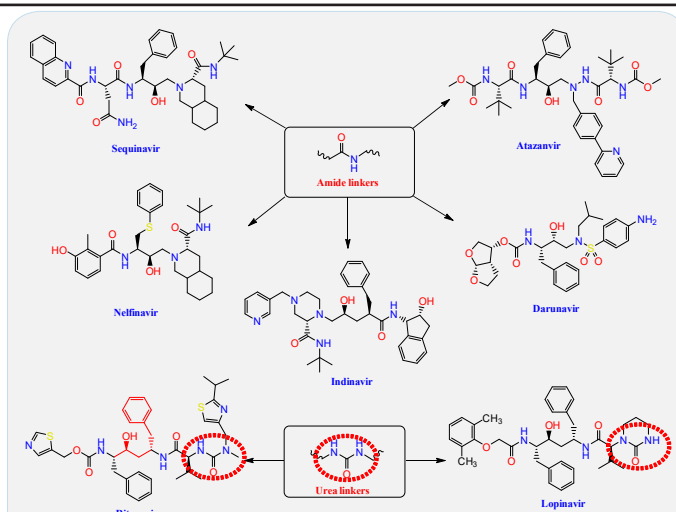


**Figure 1:** Structures of some *HIV-1* protease inhibitors containing the pharmacophoric amide and urea fragments.

Our rational depends on that VEGFR-2 inhibitors represent the main pharmacophoric urea and/or amide linkers (Figure 2).
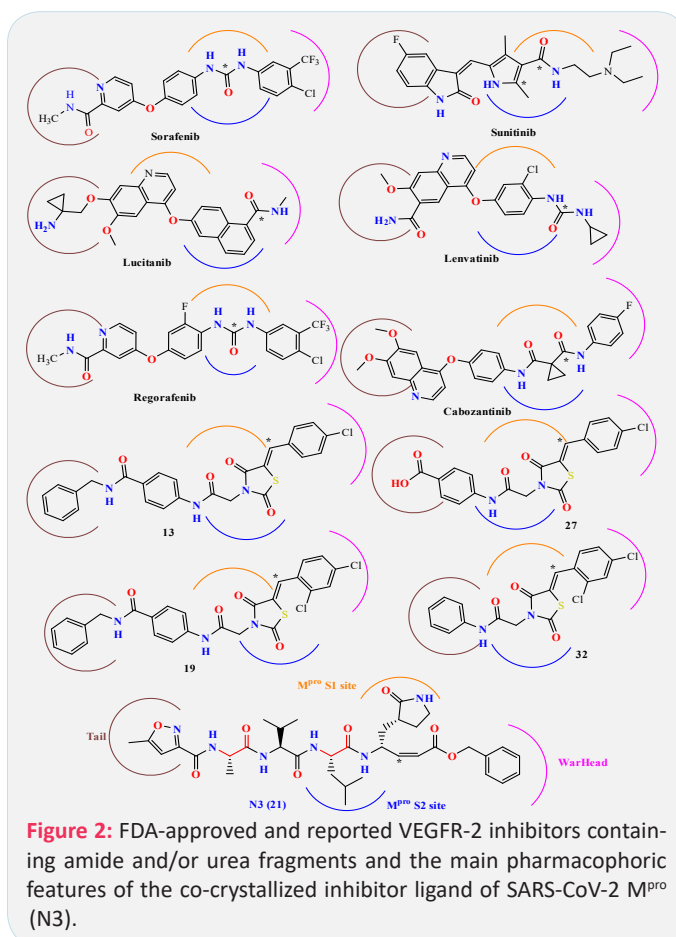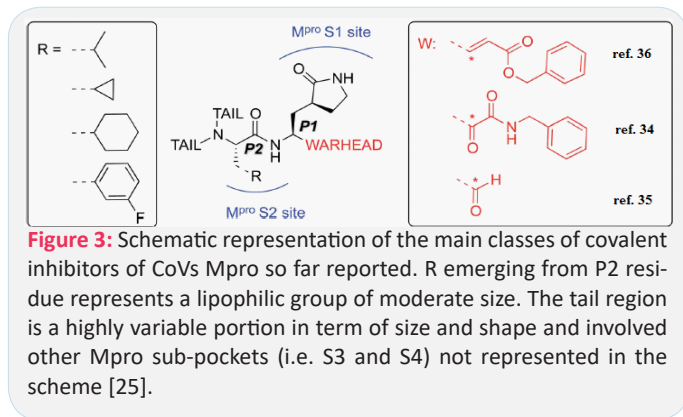


**Figure 2:** FDA-approved and reported VEGFR-2 inhibitors containing amide and/or urea fragments and the main pharmacophoric features of the co-crystallized inhibitor ligand of SARS-CoV-2 $M^{pro}$ (N3).

Our rational also depends on simulation of the inhibition process of SARSCoV-2 $M^{pro}$ with N3. There are many N3-analogues as potential inhibitors, in which the recognition and warhead motifs are modified (Figures 2 & 3). QM/MM modeling of the mechanism of inhibition of $M^{pro}$ by these compounds indicates that they may act as irreversible inhibitors and/or as a potential reversible inhibitor [25].
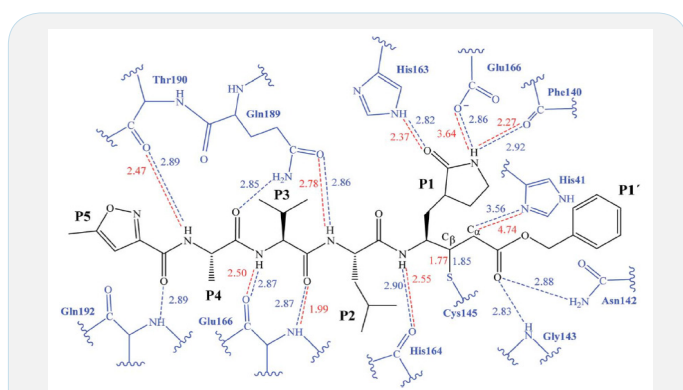
The best characterized $M^{pro}$ inhibitors so far act with a covalent mechanism. They share a similar recognition moiety, i.e. a peptidomimetic scaffold of moderate size at the P1 position and a branched lipophilic group at P2 [26-28] and are equipped with a reactive warhead (Figures 2 & 3). Warheads so far em-

ployed for the design of SARS-CoV-2 inhibitors ranged from classical Michael acceptors (MAs) to activated carbonyl derivatives. Compounds equipped with less reactive warheads (i.e. carbonyl based compounds or nitriles) act as reversible inhibitors, as they form metastable adducts with cysteine residues. In terms of target engagement, duration of inhibition and efficacy, MAs have important potential advantages over other warheads [29].
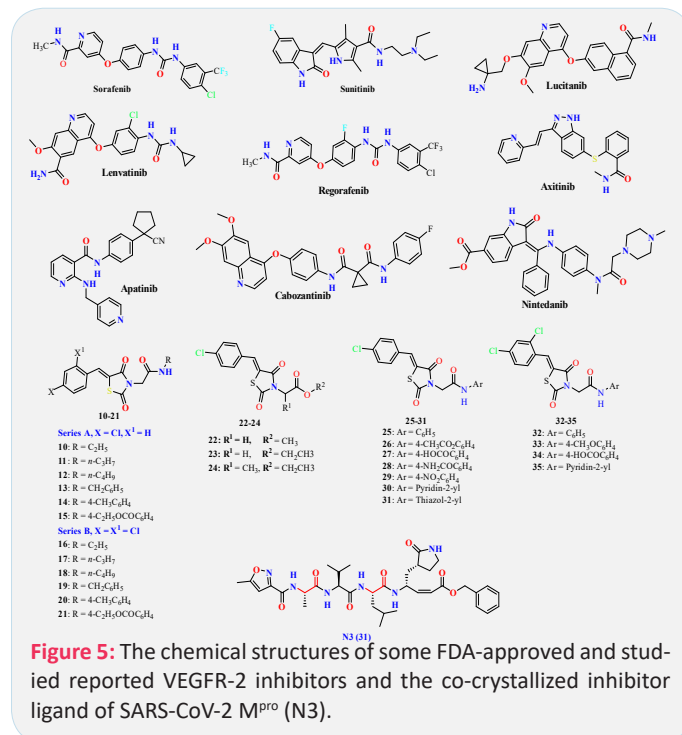
In this research our derivatives are expected to be covalent inhibitors of SARS-CoV-2 as N3 specially thiazolidine2,4-dione derivatives and sunitinib were expected to be classical Michael acceptors (MAs).



**Figure 3:** Schematic representation of the main classes of covalent inhibitors of CoVs Mpro so far reported. R emerging from P2 residue represents a lipophilic group of moderate size. The tail region is a highly variable portion in term of size and shape and involved other Mpro sub-pockets (i.e. S3 and S4) not represented in the scheme [25].

The first step of our program towards the design of new SARSCoV M$^{pro}$ inhibitors was the study of the reaction with the N3 inhibitor originally proposed by Yang et al [30]. A schematic representation of the equilibrated structure of the active site is shown in Figure 4, where important interactions found in the MD simulations and the X-ray structure obtained by Jin et al [31] are indicated as blue and red dashed lines, respectively. The pattern of interactions between the enzyme and the inhibitor in our equilibrated structure is quite close to that observed crystallographically, thus supporting our starting structure for the exploration of the full mechanism. The MD results confirm the absence of hydrogen bond interactions with some of the side chains of the residues of N3 (P2–P5) which, considering the demonstrated efficiency of this inhibitor, can be used as a guide for the design of improved compounds not requiring hydrogen bond interactions with these sites as mentioned by Arafet et al [25].



**Figure 4:** Schematic representation of N3 in the active site of SARS-CoV-2 M$^{pro}$. The dashed lines indicate hydrogen bond interactions between the inhibitor the protein found in MD simulations (blue lines) and the X-ray structure (red lines) obtained by Jin et al [31]. Interatomic distances, computed as average values over the MD simulations (in blue) and from the X-ray structure (in red), are reported in Å.

On the other hand, the FDA-approved VEGFR-2 inhibitors (e.g. sorafinib containing urea linkers [32] and sunitinib containing amide linker [33]) and our studied and reported thiazolidine2,4-dione derivatives as VEGFR-2 inhibitors [34,35]) have structure similarity to HIV-1 protease inhibitors and/or the main pharmacophoric features of the co-crystallized inhibitor ligand of SARS-CoV-2 M$^{pro}$ (N3) (Figure 5). So, the main objective of this study is to determine the efficiency of most VEGFR-2 inhibitors against SARS-CoV-2 using *in silico* docking and Molecular Dynamics (MD) simulation approaches. Besides, the studied VEGFR-2 inhibitors can be used as lead compounds for further optimization in the future based on SAR studied attaining better activity against SARS-CoV-2 M$^{pro}$.



**Figure 5:** The chemical structures of some FDA-approved and studied reported VEGFR-2 inhibitors and the co-crystallized inhibitor ligand of SARS-CoV-2 M$^{pro}$ (N3).

## Results and discussion

### Molecular docking studies

COVID-19 virus M$^{pro}$ has a Cys–His catalytic dyad, and the substrate-binding site is located in a cleft between domain I and II. The N3 inhibitor is fitted inside the substrate-binding pocket of COVID-19 virus M$^{pro}$ showing asymmetric unit containing only one polypeptide. Molecular docking simulation of VEGFR-2 inhibitors (1-35) and N3 inhibitor 36 into M$^{pro}$ active site was done.

The docked results were compared to the crystal structure of the bound ligand–protein complex. The obtained success rates were highly excellent as cited in Table 1. The N3 ligand was docked into M$^{pro}$ active site (pdb code: 6LU7). The RMSD of the docked ligand was 0.98 Å as it seems exactly superimposed on the native bound one (Figure 6). These results indicated the high accuracy of the docking simulation.
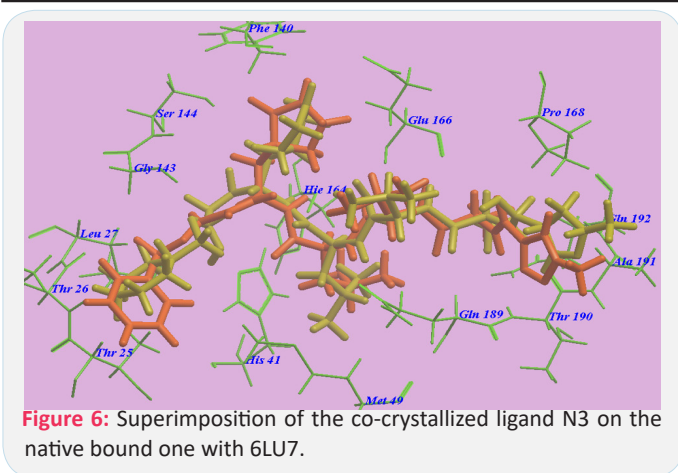
**Figure 6:** Superimposition of the co-crystallized ligand N3 on the native bound one with 6LU7.

The proposed binding mode of N3 is highly matched with that obtained by Jin et al and exhibited eight H-bonds. It formed two H-bonds with GLU166 (1.80 Å and 1.94 Å), one H-bond with SER144 (1.70 Å), one H-bond with GLY143 (2.22 Å), one H-bond with PHE140 (2.43 Å), one H-bond with HIE164 (2.76 Å), one H-bond with GLN189 (2.33 Å) and one H-bond with THR190 (2.22 Å). Moreover, it was confirmed to form many hydrophobic interactions as it occupied different hydrophobic groves as shown in Figure 7.

**Table 1:** Receptor interactions and binding energies of the identified VEGFR-2 inhibitors into the N3 inhibitor binding site of COVID-19 main protease.

| Ligand | Binding energy (kcal/mol) | Interacting amino acids | | Distance Å |
|---|---|---|---|---|
| Sorafenib | -8.0 | CYS 145 | H-donor | 4.47 |
| | | CYS 145 | H-donor | 3.98 |
| | | ASN 142 | H-donor | 2.98 |
| Sunitinib | -7.5 | CYS 145 | H-donor | 3.40 |
| | | GLY 143 | H-acceptor | 3.11 |
| Lucitanib | -8.0 | GLU 166 | H-donor | 3.21 |
| | | GLU 166 | H-donor | 3.09 |
| Lenvatinib | -8.3 | ASN 142 | H-acceptor | 3.56 |
| Regorafenib | -7.5 | CYS 145 | H-donor | 4.15 |
| | | CYS 145 | H-donor | 3.88 |
| Axitinib | -7.4 | ----- | ---- | --- |
| Apatinib | -7.5 | CYS 145 | H-donor | 3.45 |
| | | MET 165 | pi-H | 3.74 |
| | | MET 165 | pi-H | 3.67 |
| Cabozantinib | -8.1 | MET 165 | H-donor | 3.72 |
| | | THR 190 | H-donor | 3.52 |
| | | GLU 166 | H-acceptor | 2.98 |
| | | THR 26 | pi-H | 4.69 |
| Nintedanib | -7.7 | THR 26 | H-donor | 3.34 |
| | | ASN 142 | H-acceptor | 2.98 |
| 10 | -7.2 | ASN 142 | H-donor | 3.49 |
| | | MET 165 | H-donor | 3.66 |
| | | CYS 145 | H-acceptor | 3.08 |
| 11 | -7.1 | ASN 142 | H-donor | 3.55 |
| | | GLU 166 | H-donor | 2.84 |
| | | CYS 145 | H-acceptor | 3.03 |
| | | GLU 166 | pi-H | 4.31 |
| 12 | -7.0 | ASN 142 | H-donor | 3.39 |
| | | GLU 166 | H-donor | 2.94 |
| | | CYS 145 | H-acceptor | 3.02 |
| | | GLU 166 | pi-H | 4.27 |
| 13 | -8.1 | CYS 145 | H-donor | 3.08 |
| | | THR 25 | pi-H | 4.17 |
| 14 | -7.4 | CYS 145 | H-donor | 3.38 |
| | | CYS 145 | H- donor | 3.57 |
| | | HIE 41 | H-acceptor | 3.16 |
| | | GLU 143 | pi-H | 4.50 |
| 15 | -7.4 | GLN 189 | H-donor | 3.01 |
| | | GLY 143 | H-acceptor | 2.94 |
| | | GLU 166 | H-acceptor | 2.95 |
| 16 | -7.4 | GLN 189 | H-donor | 2.95 |
| | | GLY 143 | H- acceptor | 2.96 |
| | | GLU 166 | H-acceptor | 2.87 |
| 17 | -7.4 | HIP 164 | H-donor | 3.37 |
| | | THR 24 | H-donor | 3.03 |
| | | ASN 142 | H-acceptor | 3.48 |
| 18 | -7.3 | ASN 142 | H-donor | 3.53 |
| | | CYS 145 | H-donor | 2.95 |
| | | GLU 166 | H-acceptor | 4.17 |
| 19 | -8.1 | THR 26 | H-donor | 3.66 |
| | | ASN 119 | H-donor | 3.25 |
| | | TYR 118 | pi-pi | 3.90 |
| 20 | -7.2 | ASN 142 | H-donor | 3.56 |
| | | CYS 145 | H-acceptor | 3.07 |
| | | GLU 166 | pi-H | 4.31 |
| 21 | -7.3 | CYS 145 | H-donor | 4.43 |
| | | GLU 166 | H- donor | 3.52 |
| | | THR 25 | pi-H | 4.14 |
| 22 | -6.2 | CYS 145 | H- donor | 3.66 |
| | | GLY 143 | H-acceptor | 2.80 |
| 23 | -6.3 | GLY 143 | H- acceptor | 2.86 |
| | | SER 144 | H-acceptor | 2.75 |
| 24 | -6.1 | ---- | ---- | ---- |
| 25 | -7.4 | CYS 145 | H-donor | 3.31 |
| | | CYS 145 | H- donor | 3.63 |
| | | CYS 145 | H- donor | 3.97 |
| | | HIE 41 | H-acceptor | 3.06 |
| 26 | -7.4 | HIP 164 | H-donor | 2.98 |
| 27 | -7.0 | GLU 166 | H-donor | 2.93 |
| | | GLU 166 | H-acceptor | 3.00 |
| 28 | -7.4 | LEU 141 | H-donor | 3.65 |
| | | ARG 188 | H-donor | 2.70 |
| | | THR 24 | H-donor | 3.96 |
| | | GLU 166 | H-acceptor | 3.28 |
| | | GLN 189 | pi-H | 4.61 |
| 29 | -7.2 | LEU 141 | H-donor | 3.66 |
| | | THR 24 | H-donor | 3.92 |
| | | THR 190 | H-donor | 2.97 |
| | | GLU 166 | H-acceptor | 3.31 |
| | | GLN 189 | pi-H | 4.61 |
| 30 | -7.3 | HIP 164 | H-donor | 3.38 |
| | | SER 46 | H-acceptor | 2.96 |
| 31 | -7.2 | CYS 145 | H-donor | 3.46 |
| | | CYS 145 | H-donor | 3.48 |
| | | CYS 145 | H-donor | 4.02 |
| | | HIE 41 | H-acceptor | 3.15 |
| 32 | -8.1 | CYS 145 | H-donor | 3.50 |
| | | CYS 145 | H-donor | 3.59 |
| | | CYS 145 | H-donor | 3.97 |
| | | HIE 41 | H-acceptor | 3.15 |
| | | THR 26 | pi-H | 4.59 |
| 33 | -7.3 | LEU 141 | H-donor | 3.78 |
| | | THR 24 | H-donor | 3.62 |
| | | GLU 166 | H-acceptor | 3.13 |
| 34 | -7.4 | LEU 141 | H-donor | 3.71 |
| | | GLU 166 | H-donor | 3.74 |
| | | HIE 41 | H-donor | 3.73 |
| | | THR 26 | H-acceptor | 3.13 |
| 35 | -7.3 | LEU 141 | H-donor | 3.80 |
| | | GLN 189 | H-donor | 3.21 |
| | | THR 143 | H-donor | 3.71 |
| | | GLU 166 | H-acceptor | 3.22 |
| | | GLN 189 | pi-H | 4.58 |
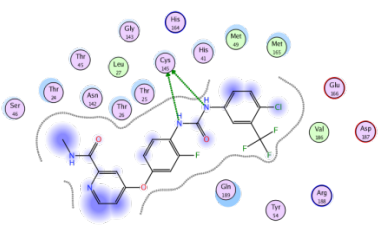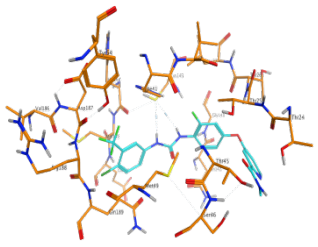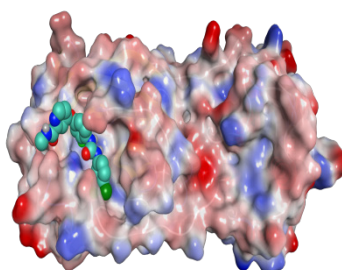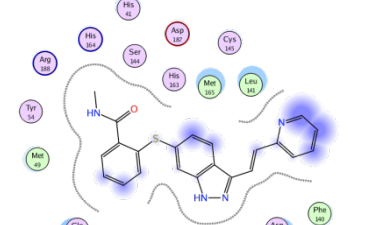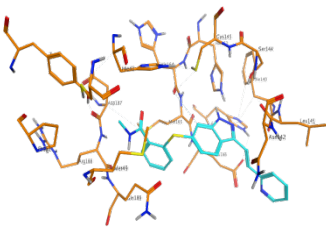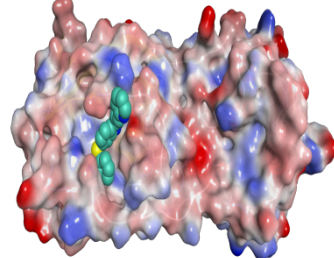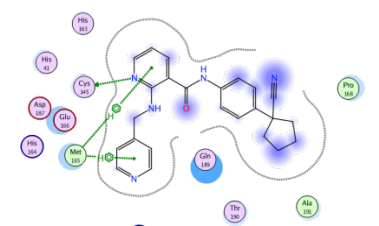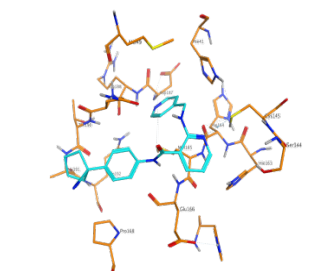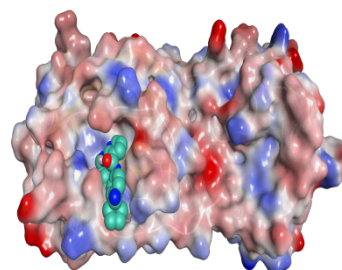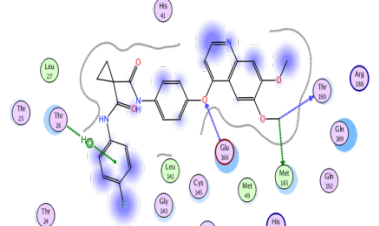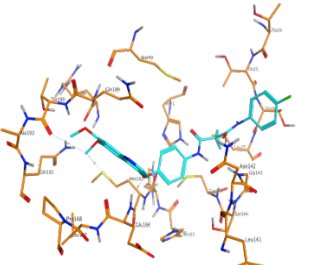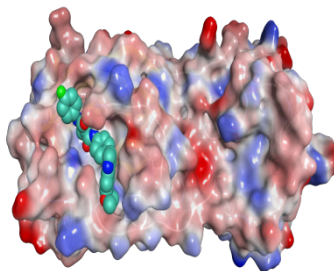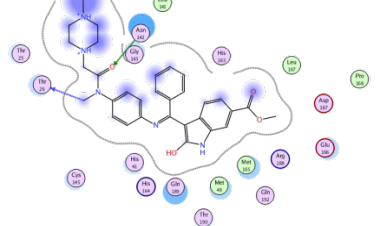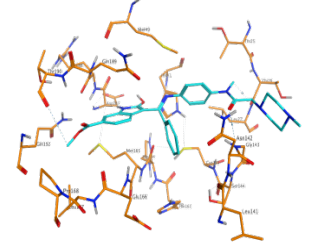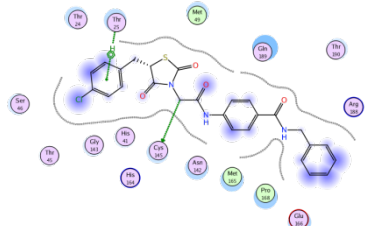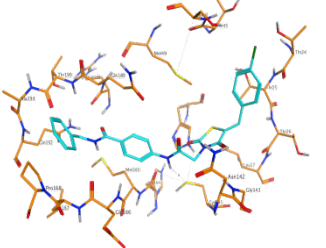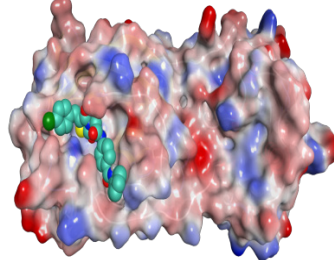
Finally, some VEGFR-2 inhibitors have excellent binding scores (-7.5 to -8.3) which are equipotent or better than the native ligand N3 (-8.1).
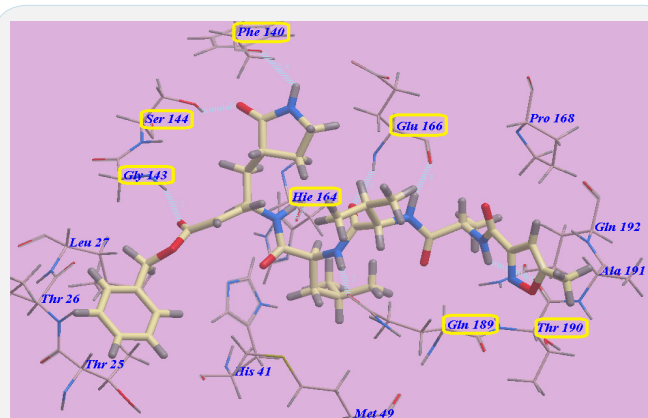
**Figure 7:** Superimposition of some docked compounds inside the binding pocket of 6LU7.

Most compounds showed nearly binding modes like the N3 inhibitor. Many poses were obtained with better binding modes and interactions inside the receptor pocket. The poses with the most acceptable scores (related to the stability of the pose) and rmsd_refine values (related to the closeness of the selected pose to the original ligand position inside the receptor pocket) were selected. The docked compounds got stabilized at the N3-binding site of M$^{pro}$ by variable several electrostatic bonds (Table 2). Results of energies and different interactions with amino acids of M$^{pro}$ protein pocket are shown in Table 1.



High-resolution crystal structures of coronavirus target explain **Sorafenib** in the active pocket (PDB ID: 6LU7, RMSD = 1.777)



High-resolution crystal structures of coronavirus target explain **Sunitinib** in the active pocket (PDB ID: 6LU7, RMSD = 2.032)
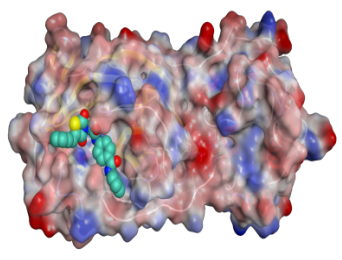


High-resolution crystal structures of coronavirus target explain **Lucitanib** in the active pocket (PDB ID: 6LU7, RMSD = 1.918)



High-resolution crystal structures of coronavirus target explain Lenvatinib in the active pocket (PDB ID: 6LU7, RMSD = 0.904)

High-resolution crystal structures of coronavirus target explain Regorafenib in the active pocket (PDB ID: 6LU7, RMSD = 1.879)



High-resolution crystal structures of coronavirus target explain Axitinib in the active pocket (PDB ID: 6LU7, RMSD = 1.412)



High-resolution crystal structures of coronavirus target explain Apatinib in the active pocket (PDB ID: 6LU7, RMSD = 1.864)



High-resolution crystal structures of coronavirus target explain Cabozantinib in the active pocket (PDB ID: 6LU7, RMSD = 1.859)



High-resolution crystal structures of coronavirus target explain Nintedanib in the active pocket (PDB ID: 6LU7, RMSD = 1.725)

| | High-resolution crystal structures of coronavirus target explain compound 13 in the active pocket (PDB ID: 6LU7, RMSD = 2.633) | | |
|---|---|---|---|
| 19 |  | | |
| | High-resolution crystal structures of coronavirus target explain compound 19 in the active pocket (PDB ID: 6LU7, RMSD = 1.999) | | |
| 32 |  | | |
| | High-resolution crystal structures of coronavirus target explain compound 32 in the active pocket (PDB ID: 6LU7, RMSD = 1.948) | | |

**Figure 8:** 2 D, 3 D, and surface and maps representations of the best poses of VEGFR-2 inhibitors against the binding site of the SARS-CoV-2 M[pro] protein, 6LU7.

**N.B**: The surface and maps representations show the H-bond donor, H-bond acceptor, and hydrophobic regions around the docked compound.
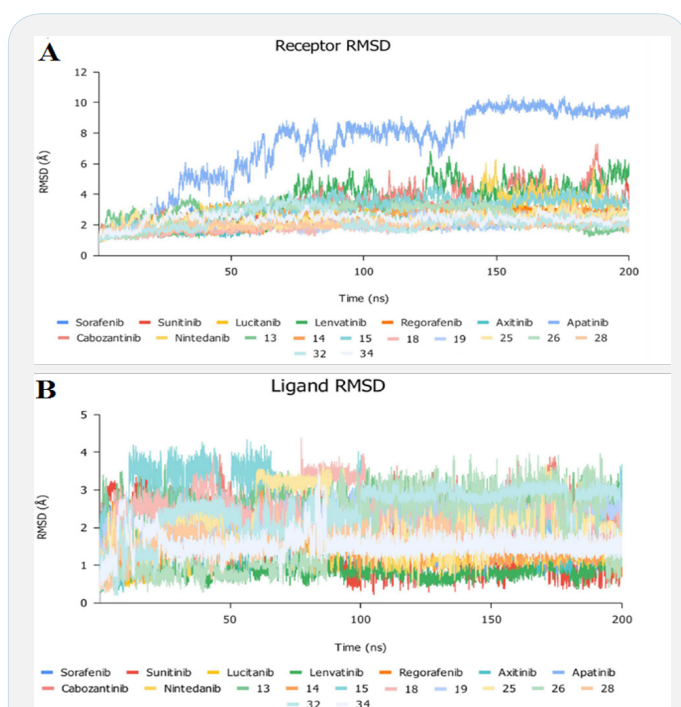


**Figure 9:** Analysis of RMSD trajectories for the ligand-Mpro protein complexes throughout 200 ns all-atom MD simulation. **(A)** protein RMSD; **(B)** ligand RMSD, relative to backbone versus MD simulation time in nanoseconds.

### Binding-free energy calculations

The binding-free energy calculation was performed to understand the nature of ligand–protein interaction as well as obtain more detailed information concerning the individual ligand contribution [39]. In this regard, the molecular mechanics generalized Born surface area (MM/GBSA) calculation was implemented for binding-free energy estimation, where higher negative binding energy explains more ligand affinity towards its respective target pocket [40]. Utilizing implicit solvent models in MM/GBSA framework allows for efficient calculations without significant loss of accuracy. MM/GBSA demonstrated accurate pose prediction on a large benchmark of protein–ligand complexes with non-redundant binding poses [41]. Adopting the calculation across the 200 ns MD simulation time course was rationalized by the rapidly attained equilibration/convergence of the complex RMSD trajectories following few initial MD frames. To our delight, compounds Lenvatinib (4), Nintedanib (9), 28 and 32 as VEGFR-2 inhibitors bound to SARS-CoV-2 M[pro] target have depicted significant free binding and affinity to target's pocket (Table 2) (Figure 10). Dissecting the obtained binding-free energy into its contributing energy terms, the van der Waal interactions showed superior contribution within the free-binding energy calculation of ligand–protein complex as compared to electrostatic potential energy except in case of sorafenib. Moreover, Gas-phase energy ($\Delta G_{gas}$) of the solute is the summation of internal energies, vander Waals energies and electrostatic energies ($\Delta G_{gas}$ = VDWAALS + EEL). The solvation-free energy, $\Delta G_{solv}$, is broken into the polar and non-polar components $\Delta G_{solv} = \Delta G_{pol} + \Delta G_{nonpol}$ and then $\Delta$Total = $\Delta$Ggas + $\Delta$Gsolv. N3 exhibited higher both $\Delta G_{gas}$ and $\Delta G_{solv}$ compared to our VEGFR-2 inhibitors except in case of Lenvatinib, Nintedanib, compounds 28, and 32 which showed the highest $\Delta$Gsolv. Based on current literature, the M[pro] pocket is considered of more hydrophobic in nature for being deep, less solvent exposed, and with conserved hydrophobic pocket lining residues. Being hydrophobic and with large surface area, the M[pro] binding site could favour higher nonpolar interactions with N3 where the latter attained a more extended conformation within the target's pocket. Finally, similar binding pattern was depicted for Lenvatinib (4), Nintedanib (9) and 32 across the docking and MD simulation study. Compounds Lenvatinib (4) and Nintedanib (9), 28 and 32 exhibited more preferential free-binding energy as

compared to N3 at M$^{pro}$ binding site, the thing that confirms its superior target affinity over N3 within the preliminary docking analysis. It worth to not that the profound free-binding energy of the top-stable VEGFR-2 inhibitors correlates well with the obtained initial docking score ranking (Table 1).

**Table 2:** Average of total binding-free energies and individual energy term concerning the promising VEGFR-2 inhibitors compounds and reference N3 at Mpro protein binding sites.

| Ligand | VDWAALS | EEL | ΔG gas | ΔG solv | ΔTotal | Standard Error |
|---|---|---|---|---|---|---|
| Sorafenib | -24.1 | -13.0 | -37.1 | 20.2 | -16.9 | 0.16 |
| Sunitinib | -25.7 | -17.9 | -43.6 | 26.2 | -17.4 | 0.15 |
| Lucitanib | -31.9 | -10.0 | -41.9 | 23.7 | -18.2 | 0.09 |
| Lenvatinib | -44.8 | -20.2 | -65.0 | 33.0 | -32.0 | 0.07 |
| Regorafenib | -31.7 | -14.7 | -46.4 | 26.5 | -19.9 | 0.04 |
| Axitinib | -47.3 | -15.6 | -62.9 | 33.3 | -29.6 | 0.04 |
| Apatinib | -31.3 | -12.6 | -43.9 | 27.4 | -16.5 | 0.06 |
| Cabozantinib | -34.6 | -12.3 | -46.9 | 25.6 | -21.3 | 0.07 |
| Nintedanib | -61.5 | -15.0 | -76.5 | 38.5 | -38.0 | 0.05 |
| 13 | -42.9 | -13.3 | -56.2 | 26.2 | -30.0 | 0.05 |
| 14 | -40.2 | -15.9 | -56.1 | 28.3 | -27.8 | 0.06 |
| 15 | -31.0 | -14.0 | -45.0 | 23.5 | -21.5 | 0.09 |
| 18 | -35.8 | -14.1 | -49.9 | 23.3 | -26.6 | 0.07 |
| 19 | -42.4 | -15.1 | -57.5 | 28.9 | -28.6 | 0.07 |
| 25 | -10.7 | -3.8 | -14.5 | 7.0 | -7.5 | 0.11 |
| 26 | -15.0 | -6.1 | -21.1 | 11.2 | -9.9 | 0.10 |
| 28 | -44.5 | -25.7 | -70.2 | 36.5 | -33.7 | 0.05 |
| 32 | -46.7 | -16.6 | -63.3 | 26.5 | -36.8 | 0.04 |
| 34 | -22.1 | -65.1 | -87.2 | 65.2 | -22.0 | 0.04 |
| N3 | - 45.6 | - 23.2 | - 68.8 | 37.6 | - 31.2 | 0.04 |
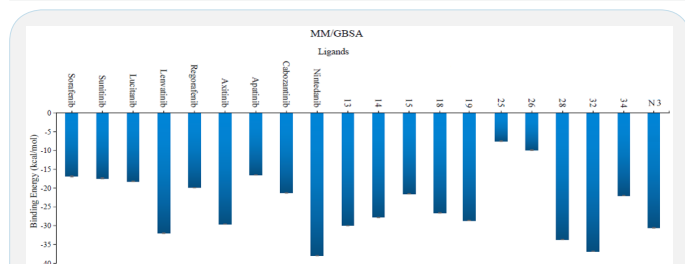


**Figure 10:** Analysis of RMSD trajectories for the ligand-Mpro protein complexes throughout 200 ns all-atom MD simulation. **(A)** protein RMSD; **(B)** ligand RMSD, relative to backbone versus MD simulation time in nanoseconds.

### Conclusion

The present study suggests the potential anti-SARS-CoV-2 activities of thirty five reported VEGFR-2 inhibitors containing the amide and urea linkers. In our derivatives all thiazolidine2,4-dione derivatives are expected to be Michael acceptors and are covalent inhibitors of SARS-CoV-2. Nineteen members revealed the best *in silico* results [1-9, 13-15, 18, 19, 25, 26, 28, 32 and 34] and hence, were subjected to further MD simulation for their inhibitory activities against SARS-CoV-2 M$^{pro}$ across the 200 ns. The molecular mechanics generalized Born surface area (MM/GBSA) calculation was implemented for binding-free energy estimation. Both compounds Lenvatinib (4), Nintedanib (9), 28 and 32 as VEGFR-2 inhibitors bound to SARS-CoV-2 M$^{pro}$ target have depicted significant free binding and affinity to target's pocket. These results greatly confirmed our proposed rational and agreed with our computational findings through molecular docking (targeting the viral M$^{pro}$) and molecular dynamics which consequently suggest the strong expected activities for the other studied and discussed VEGFR-2 inhibitors as well. So, we recommend further preclinical and clinical studies for the fast repurposing of the reported, already found and discussed FDA-approved VEGFR-2 inhibitors as proposed candidates for the management of Covid-19 viral pandemic. Additionally, the studied medications can deal with as promising lead compounds for further structural modifications to enhance their activity against SARS-CoV-2.

### Materials and methods

For molecular docking studies we used *AutoDock* Tools software [42] and molesoft program [34]. We used the Amber 18 molecular dynamics package [43] together with the force field AMBERff14SB for the protein [44], and the GAFF2 force field for the ligands [45]. The co-crystallized inhibitor ligand (N3) was used as a reference standard.

**Preparation of the tested VEGFR-2 inhibitors**

Structures of the tested compounds and the formal charges on atoms were checked by 2D depiction, subjected to energy minimization and the partial charges were automatically calculated. The tested compounds together with the co-crystallized ligand (N3) were imported in the same database and saved in the form of MDB file for the docking calculations with target

protease as described earlier [46].

### Preparation of the target (SARS-CoV-2 M$^{pro}$)

Protein Data Bank was used to download the crystal structure of SARS-CoV-2 M$^{pro}$ with (PDB code: 6LU7and resolution: 2.16 Å) [47]. The crystal structure was protonated, hydrogen atoms were added with their standard 3D geometry, automatic correction for any errors in the atom's connection and type was applied, and potential fixation of the receptor and its atoms were done. Site Finder was applied for selection of the same active site of co-crystallized inhibitor using all default items and dummy atoms of the pocket were created [48].

### Docking of the tested VEGFR-2 inhibitors to the viral M$^{pro}$ binding site

Docking of the previously prepared database composed of the tested thirty five VEGFR-2 inhibitors (1-35) and the co-crystallized inhibitor N3 (36) was performed. The following methodology was applied: the file of the prepared active site was loaded, and general docking process was initiated. The program specifications were adjusted so that the docking site (dummy atoms), the placement methodology (triangle matcher) and the scoring methodology (London dG). Rigid receptor as refinement methodology and GBVI/WSA dG as the scoring methodology for selection of the best ten poses from one hundred different poses for each tested compound [49]. The MDB file of the thirty ligands was loaded and general dock calculations were run automatically. The obtained poses were studied after completion, and the best ones having the best ligand–enzyme interactions and the most acceptable root mean square deviation (rmsd) values were selected and stored for energy calculations. At the beginning, a validation process was also performed for the target receptor by docking only the co-crystallized ligand and low RMSD values between docked and crystal conformations indicate a valid performance [50,51].

### Molecular dynamics (MD) simulation

The top ninety ranked score complexes were processed to a molecular dynamics study to address their binding affinity to the protease enzyme. The N3 compound was also used in the docking and the simulation as a positive control. Ligand force fields were generated using GAFF2 [45] and the force field AMBERff14SB for the protein [44]. The complex was solvated expanding 15.0 Å in each direction with TIP3P water box of octahedral truncated box neutralized to a salt concentration of 150 mM of NaCl. The system was prepared *via* multiple energy minimization, equilibration and production steps under gradual decline position restraints on the ligand and protein achieving 310 K of temperature and 1.0 bar of pressure followed by a restraint-free production run of 200 ns. The coordinates saved every 2 ns. The binding energy between the ligand and the receptor was determined by applying MM/GBSA approach on the trajectory using MM/PBSA.py script of Amber [52], the calculations were for the last 50 ns using snapshots of 1 ns intervals from the simulation trajectory.

**Conflicts of interest:** The authors declare no conflict of interest.

### References

1. Abbruzzese C, Matteoni S, Persico M, Villani V, Paggi MG. Repurposing chlorpromazine in the treatment of glioblastoma multiforme: analysis of literature and forthcoming steps. J Exp Clin Cancer Res. 2020; 39: 26.

2. Elfiky AA. Anti-HCV, nucleotide inhibitors, repurposing against COVID-19. Life Sci. 2020; 248: 117477.

3. Zhou Y, Hou Y, Shen J, Huang Y, Martin W, Cheng F. Network-based drug repurposing for novel coronavirus 2019-nCoV/SARS-CoV-2. Cell Discov. 2020; 6:14.

4. Baron SA, Devaux C, Colson P, Raoult D, Rolain JM. Teicoplanin: an alternative drug for the treatment of coronavirus COVID-19? Int J Antimicrob Agents. 2020;105944.

5. Fan HH, Wang LQ, Liu WL, An XP, Liu ZD, He XQ, et al. Repurposing of clinically approved drugs for treatment of coronavirus disease 2019 in a 2019-novel coronavirus (2019-nCoV) related coronavirus model. Chin Med J. 2020.

6. Li G, De Clercq E. Therapeutic options for the 2019 novel coronavirus (2019-nCoV). Nat Rev Drug Discov. 2020; 19: 149-150.

7. Chen YW, Yiu CB, Wong KY. Prediction of the SARS-CoV-2 (2019-nCoV) 3Clike protease (3CL (pro)) structure: virtual screening reveals velpatasvir, ledipasvir, and other drug repurposing candidates. F1000Res. 2020; 9: 129.

8. de Wit E. Prophylactic and therapeutic remdesivir (GS-5734) treatment in the rhesus macaque model of MERS-CoV infection. Proceedings of the National Academy of Sciences. 2020; 117: 6771-6776.

9. Wu F. A new coronavirus associated with human respiratory disease in China. Nature. 2020; 579: 265-269.

10. Chen Y, Liu Q, Guo D. Emerging coronaviruses: genome structure, replication, and pathogenesis. Journal of medical virology. 2020; 92: 418-423.

11. Anand K. Coronavirus main proteinase (3CLpro) structure: basis for design of anti-SARS drugs. Science. 2003; 300: 1763-1767.

12. Elzupir AO. Inhibition of SARS-CoV-2 main protease 3CLpro by means of α-ketoamide and pyridone-containing pharmaceuticals using in silico molecular docking. Journal of molecular structure. 2020;1222: 128878.

13. Elmaaty AA. Revisiting activity of some glucocorticoids as a potential inhibitor of SARS-CoV-2 main protease: theoretical study. RSC Advances. 2021; 11: 10027-10042.

14. Elmaaty AA. et al. In a search for potential drug candidates for combating COVID-19: computational study revealed salvianolic acid B as a potential therapeutic targeting 3CLpro and spike proteins. Journal of Biomolecular Structure and Dynamics. 2021; 1-28.

15. Soltane R. Strong Inhibitory Activity and Action Modes of Synthetic Maslinic Acid Derivative on Highly Pathogenic Coronaviruses: COVID-19 Drug Candidate. Pathogens. 2021; 10: 623.

16. Zaki AA. Molecular docking reveals the potential of Cleome amblyocarpa isolated compounds to inhibit COVID-19 virus main protease. 2020; 44: 16752-16758.

17. Zaki AA. Calendulaglycoside A Showing Potential Activity Against SARS-CoV-2 Main Protease: Molecular Docking, Molecular Dynamics, and SAR Studies. Journal of Traditional and Complementary Medicine. 2021.

18. Alnajjar R. Molecular docking, molecular dynamics, and in vitro studies reveal the potential of angiotensin II receptor blockers to inhibit the COVID-19 main protease. 2020; 6: e05641.

19. Nicola M. Health policy and leadership models during the COVID-19 pandemic-review article. International Journal of Surgery. 2020.

20. Khattab M, Al-Karmalawy AA. Revisiting Activity of Some No-

codazole Analogues as a Potential Anticancer Drugs Using Molecular Docking and DFT Calculations. Frontiers in Chemistry. 2021; 9: 92.

21. Milite C. Novel 2-substituted-benzimidazole-6-sulfonamides as carbonic anhydrase inhibitors: synthesis, biological evaluation against isoforms I, II, IX and XII and molecular docking studies. Journal of enzyme inhibition and medicinal chemistry. 2019; 34: 1697-1710.

22. Yamamoto N. HIV protease inhibitor nelfinavir inhibits replication of SARS-associated coronavirus. Biochemical and biophysical research communications. 2004; 318: 719-725.

23. Li JY. The epidemic of 2019-novel-coronavirus (2019-nCoV) pneumonia and insights for emerging infectious diseases in the future. Microbes and infection. 2020; 22: 80-85.

24. Wilson CO. Wilson and Gisvold's textbook of organic medicinal and pharmaceutical chemistry/edited by John H. Block, John M. Beale Jr: Philadelphia: Lippincott Williams & Wilkins. 2004.

25. Arafet K, Serrano-Aparicio N, Lodola A, Mulholland AJ, Gonz´alez FV, et al. Mechanism of inhibition of SARS-CoV-2 Mpro by N3 peptidyl Michael acceptor explained by QM/MM simulations and design of new derivatives with tunable chemical reactivity. Chem Sci. 2021; 12: 1433.

26. Zhang L, Lin D, Sun X, Curth U, Drosten C, et al. Crystal structure of SARS-CoV-2 main protease provides a basis for design of improved α-ketoamide inhibitors. Science. 2020; 368: 409-412.

27. Dai W, Zhang B, Jiang XM, Su H, Li J, et al. Structure-based design of antiviral drug candidates targeting the SARS-CoV-2 main protease. Science. 2020; 368: 1331-1335.

28. Z. Jin, X. Du, Y. Xu, Y. Deng, M. Liu, et al. Structure of Mpro from SARS-CoV-2 and discovery of its inhibitors. Nature. 2020; 582: 289-293.

29. Jain RP, Pettersson HI, Zhang J, Aull KD, Fortin PD, et al. Synthesis and evaluation of keto-glutamine analogues as potent inhibitors of severe acute respiratory syndrome 3CLpro. J Med Chem. 2004; 47: 6113-6116.

30. H. Yang, W. Xie, X. Xue, K. Yang, J. Ma, et al. Design of Wide-Spectrum Inhibitors Targeting Coronavirus Main Proteases. PLoS Biol. 2005; 3: e324.

31. Z. Jin, X. Du, Y. Xu, Y. Deng, M. Liu, et al. Structure of Mpro from SARS-CoV-2 and discovery of its inhibitors. Nature. 2020; 582: 289-293.

32. Wu P, Nielsen TE, Clausen MH. FDA-approved small-molecule kinase inhibitors. Trends in Pharmacological Sciences. 2015; 36: 422-439.

33. Takahashi S. Vascular endothelial growth factor (VEGF), VEGF receptors and their inhibitors for antiangiogenic tumor therapy. Biological and Pharmaceutical Bulletin. 2011; 34: 1785-1788.

34. K. El-Adl, H. Sakr, S. S. A. El-Hddad, A.-G. A. El-Helby, M. Nasser, H. S. Abulkhair, Design, synthesis, docking, ADMET profile, and anticancer evaluations of novel thiazolidine-2,4-dione derivatives as VEGFR-2 inhibitors. Arch. Pharm. 2021; e2000491.

35. El-Adl K, El-Helby A-GA, Sakr H. Design, synthesis, molecular docking, anticancer evaluations, and in silico pharmacokinetic studies of novel 5-[(4-chloro/2,4-dichloro)benzylidene]thiazolidine-2,4-dione derivatives as VEGFR-2 inhibitors. Arch Pharm. 2020; e2000279.

36. M. Karplus, Petsko GA. Molecular dynamics simulations in biology. Nature. 1990; 347: 631-639.

37. M. Arnittali, A. N. Rissanou, V. Harmandaris, Structure Of Biomolecules Through Molecular Dynamics Simulations, Procedia Computer Science. 2019; 156: 69-78.

38. Liu K, Watanabe E, Kokubo H. Exploring the stability of ligand binding modes to proteins by molecular dynamics simulations. J Comput.-Aided Mol. Des. 2017; 31: 201-211.

39. Cavasotto CN. Binding Free Energy Calculation Using Quantum Mechanics Aimed for Drug Lead Optimization. Methods Mol Biol. 2020; 2114: 257-268.

40. T. Hou, J. Wang, Y. Li, W. Wang, Assessing the Performance of the MM/PBSA and MM/GBSA Methods. 1. The Accuracy of Binding Free Energy Calculations Based on Molecular Dynamics Simulations. J Chem Inf Model. 2011; 51: 69-82.

41. N. Forouzesh, N. Mishra. An Effective MM/GBSA Protocol for Absolute Binding Free Energy Calculations: A Case Study on SARS-CoV-2 Spike Protein and the Human ACE2 Receptor. Molecules. 2021; 26: 2383.

42. Morris. AutoDock4 and AutoDockTools4: Automated docking with selective receptor flexibility. Journal of computational chemistry. 2009; 30: 2785-2791.

43. Case DA, Ben-Shalom IY, Brozell SR. AMBER 2018. San Francisco: University of California; 2018.

44. J. A. Maier, C. Martinez, K. Kasavajhala, L. Wickstrom, K. E. Hauser, C. Simmerling, ff14SB: improving the accuracy of protein side chain and backbone parameters from ff99SB. J Chem Theory Comput. 2015; 11: 3696–3713.

45. Wang J, Wolf RM, Caldwell JW, Kollman PA. Case, Development and testing of a general amber force field. J Comput Chem. 2004; 25: 1157-1174.

46. Ghanem A. Tanshinone IIA synergistically enhances the antitumor activity of doxorubicin by interfering with the PI3K/AKT/mTOR pathway and inhibition of topoisomerase II: in vitro and molecular docking studies. 2020; 44: 17374-17381.

47. Jin Z. Structure of M pro from SARS-CoV-2 and discovery of its inhibitors. Nature. 2020; 582: 289-293.

48. Eliaa SG. Empagliflozin and Doxorubicin Synergistically Inhibit the Survival of Triple-Negative Breast Cancer Cells via Interfering with the mTOR Pathway and Inhibition of Calmodulin: In Vitro and Molecular Docking Studies. ACS Pharmacology & Translational Science. 2020; 3: 1330-1338.

49. Samra RM. Bioassay-guided isolation of a new cytotoxic ceramide from Cyperus rotundus L. South African Journal of Botany. 2021; 139: 210-216.

50. Davis IW, D. Baker, RosettaLigand docking with full ligand and receptor flexibility. Journal of molecular biology. 2009; 385: 381-392.

51. McConkey BJ, Sobolev V, Edelman M. The performance of current methods in ligand–protein docking. Current Science. 2002; 845-856.

52. Miller BR, McGee TDJ, Swails JM, Homeyer N, Gohlke H, et al. Roitberg MMPBSA.py: An efficient program for end-state free energy calculations. J Chem Theory Comput. 2012; 8: 3314-3321.